Research Square

Preprints are preliminary reports that have not undergone peer review.
They should not be considered conclusive, used to inform clinical practice,
or referenced by the media as validated information.

Emulsion-forcespun hollow polymer fibers as functional sorbents for uranium removal from water

Mahmoud Firouzzare

mfirooz@aeoi.org.ir

Nuclear Science and Technology Research Institute

Roshanak Rostamian

Razi University

Research Article

Keywords: Styrene, acrylonitrile, Hollow nanofiber, Forcespinning, Amidoximation, Uranium adsorption, Emulsion spinning

Posted Date: May 30th, 2026

DOI: https://doi.org/10.21203/rs.3.rs-9707588/v1

License: This work is licensed under a Creative Commons Attribution 4.0 International License.
Read Full License

Additional Declarations: No competing interests reported.

Emulsion-forcespun hollow polymer fibers as functional sorbents for uranium removal from water

Mahmoud Firouzzare[1]***, Roshanak Rostamian***[2]

[1]*Materials and Nuclear Fuel Research School, Nuclear Science and Technology Research Institute, P.O. Box 11365-8486, Tehran, Iran*

[2] *Department of Analytical Chemistry, Faculty of Chemistry, Razi University, Kermanshah, Iran*

*Corresponding author. E-mail: mfirooz@aeoi.org.ir

Abstract

This study developed hollow amidoximated styrene–acrylonitrile (SAN) fibers using a novel emulsion-assisted solution forcespinning strategy for enhanced uranium adsorption. The fabricated hollow SAN fibers, with their unique core architecture, provided superior surface accessibility and faster mass transfer compared to solid fibers. This resulted in excellent uranium adsorption performance, achieving a maximum capacity of 190 mg g^{-1}, approximately 1.4 times higher than that of solid fibers. This work presents an innovative approach to fabricate high-performance adsorbents for efficient recovery of uranium from aqueous solutions.

Keywords Styrene–acrylonitrile. Hollow nanofiber. Forcespinning. Amidoximation. Uranium adsorption. Emulsion spinning

Introduction

Nanofibers (NFs) exhibit an exceptionally high surface-to-volume ratio, flexibility, and remarkable mechanical properties such as stiffness and tensile strength, making them highly attractive for a wide range of applications, including filtration, sensors, protective clothing, tissue engineering, the chemical peocessing, textiles, healthcare, battery separators, energy storage, and adsorption [1–3]. Conventional polymer spinning techniques such as melt, wet, dry, or gel spinning are generally unsuitable for the fabrication of nanofibers. Consequently, several advanced approaches—including self-assembly, phase separation, template synthesis, electrospinning (ES), and forcespinning (FS) —have been developed for nanofiber production [4].

FS is a relatively new fiber fabrication method that employs centrifugal force to spin nanofibers from either polymer solutions or melts. This technique is highly versatile and capable of producing nanometer-scale fibers from polymer solutions at rotational speeds up to 12,000 rpm or from polymer melts at speeds up to 25,000 rpm [5,6]. Unlike electrospinning, FS substantially reduces or completely eliminates the use of high-voltage electrical fields and large quantities of solvents, thereby offering advantages in terms of cost, safety and environmental substantially [7]. FS has successfully produced nanofibers from a wide range of polymers, including polystyrene (PS), polyacrylic acid, polycaprolactone, polyethylene oxide, polymethyl methacrylate, and polyvinylidene fluoride [8–11].

Styrene–acrylonitrile (SAN) copolymers combine the desirable characteristics of PS and polyacrylonitrile (PAN), such as high mechanical strength, transparency, chemical resistance, gloss, and oil resistance [12]. These properties make SAN a suitable material for diverse applications, including food packaging, disposable tableware, catalyst

immobilization, ultrafiltration of corrosive chemicals, and automotive components [13–15]. SAN nanofibers (SAN-NFs) also have great potential for use in separation, industrial, electrical, and biomedical applications [16].

Groundwater contamination by uranium (U) originating from nuclear waste is a major environmental challenges [17,18]. Uranium's combined chemical toxicity and radioactivity pose serious health risks [19–21]. Exposure to alpha radiation from uranium can lead to genetic damage, cancer, and other health disorders [22]. Therefore, the efficient removal and recovery of U(VI) from aqueous systems have received growing attention in recent years. Among the available treatment techniques, adsorption has been widely recognized as an effective, simple and removing heavy metals such as uranium from contaminated water [23–25].

Among various adsorbent materials, fibrous adsorbents offer distinct advantages due to their large surface area, mechanical robustness, and tunable chemical functionality. However, adsorption efficiency in solid nanofibers is often limited by slow diffusion within their dense structure. To overcome this limitation, hollow nanofiber (HNF) architectures have been developed, providing additional internal surfaces and shorter diffusion paths that facilitate faster and more efficient ion transport.

HNFs can typically be fabricated through co-axial spinning, uniaxial (emulsion-based) spinning, or chemical vapor deposition (CVD) [26–29]. The emulsion method enabled the formation of core-shell structures, in which emulsified droplets organize into distinct core and shell phases as the solvent evaporates. In this approach, fibers form via the simultaneous flow of two immiscible liquids through inner and outer capillaries [30,31].

Hollow structures are obtained by removing the core phase after spinning. Chemical modification of SAN nanofibers through amidoximation introduces strong chelating groups capable of selectively binding uranyl ions (UO_2^{2+}) via coordination and hydrogen bonding. In this context, the present study proposes a novel emulsion forcespinning approach for fabricating **amidoximated SAN hollow nanofibers (SAN-HNFs)** and systematically investigates their uranium adsorption behavior compared to that of solid SAN nanofibers (SAN-NFs). Comprehensive kinetic and isotherm studies were conducted to elucidate the adsorption mechanism, and the adsorption performance of SAN-HNFs was benchmarked against some previously reported fiber-based adsorbents.

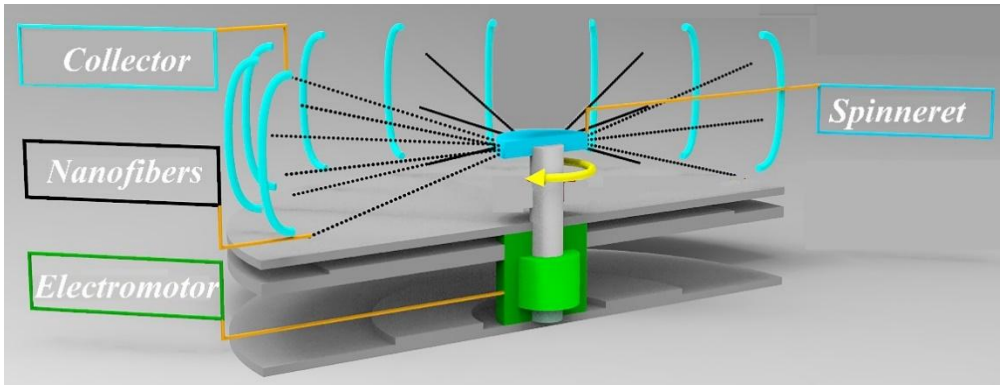
Experimental

Equipment

Nanofibers and hollow nanofibers were fabricated using a homemade forcespinning (FS) apparatus consisting of a spinneret equipped with micron-scale nozzles that eject polymer solution under centrifugal force generated by an electromotor (Scheme 1). Fibers were collected on a static metallic rod collector positioned at a fixed distance from the spinneret tip.

The morphology of the Fibers was examined using a scanning electron microscope (SEM, Zeiss Evo18, Germany). Fourier-transform infrared (FT-IR) spectra were recorded with a Bruker Vector 22 spectrometer over the range of 500–4000 cm^{-1}. Fiber diameters were measured using Digimizer image analysis software. The uranium concentrations in

solution were determined using an Optima DV 7300 inductively coupled plasma (ICP) emission spectrometer, and pH values were monitored with a Metrohm Ml 150 pH-meter.



Scheme 1 Schematic representation of the forcespinning apparatus.

Materials

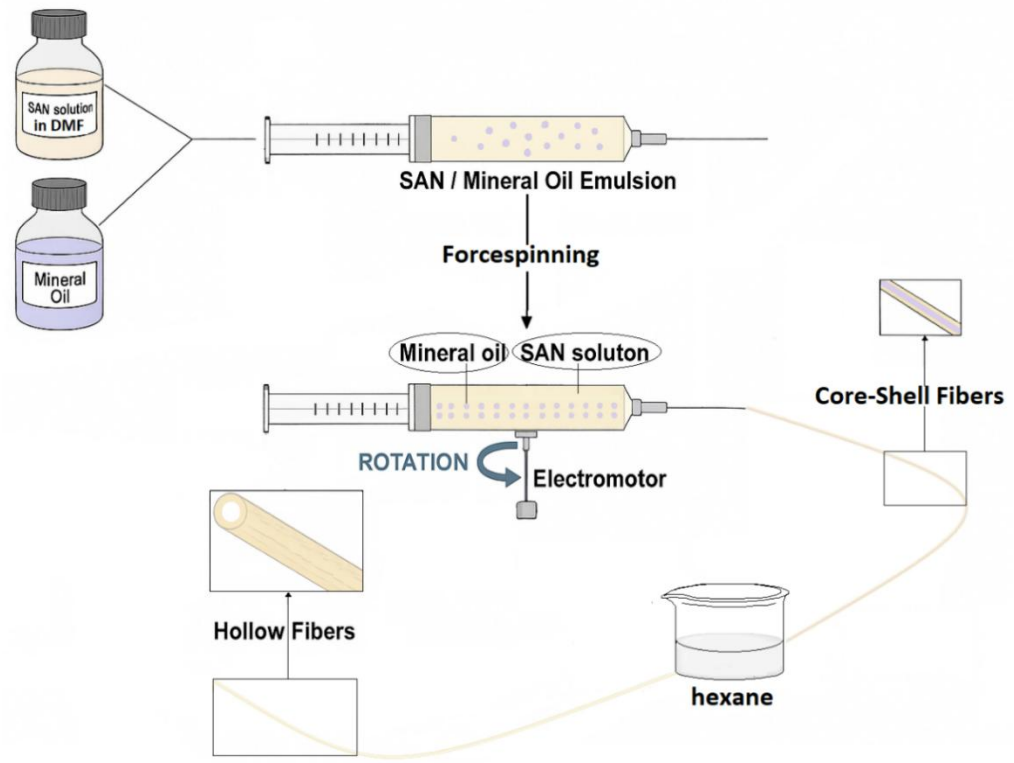
Hexane, mineral oil, dimethylformamide (DMF), uranyl nitrate hexahydrate ($UO_2(NO_3)_2 \cdot 6H_2O$), hydrochloric acid (HCl), sodium hydroxide (NaOH), and hydroxylamine hydrochloride ($NH_2OH \cdot HCl$) were purchased from Merck (Germany). Styrene-acrylonitrile (SAN) copolymer (High Flow, MFI:66) was obtained from Ghaed Basir Petrochemical Co. (Iran). All reagents were of analytical grade, and solutions were prepared using deionized water.

Preparation of SAN-NFs and SAN-HNFs

SAN solutions with various concentrations were prepared in DMF through alternating ultrasonic tretment and magnetic stirring at 50 °C until complete dissolution was achieved. SAN nanofibers (SAN-NFs) were produced via FS under systematically varied conditions.

For the preparation of hollow nanofibers (SAN-HNF), an emulsion of SAN solution and mineral oil was prepared at predetermined volume ratios and mechanically shaken for 2 h

prior to spinning. The core-shell fibers were subsequently immersed in hexane for 24 h to remove the mineral oil core, thereby yielding hollow structures (Scheme 2).



Scheme 2 Fabrication steps of hollow nanofibers via emulsion forcespinning.

Amidoximation of Fibers

Amidoximation of SAN-NFs and SAN-HNFs was performed by reacting the nitrile groups with a 10% (w/v) hydroxylamine solution at 80 °C for 72 h, with the reaction solution replaced twice during the process. The modified fibers were thoroughly washed with deionized water and dried at 50 °C for 24 h.

Adsorption Experiments

Batch adsorption experiments were conducted to investigate the effects of contact time, initial uranium concentration, and solution pH on U(VI) uptake. Prior to adsorption,

amidoximated fibers were pre-treated in 2.5% NaOH solution at 80 °C for 3 h, then filtered and washed with deionized water until neutral pH was reached.

For each test, fibers were immersed in 100 mL of uranium solution and shaken at 210 rpm at 25 °C. Samples were withdrawn and filtered at predetermined time intervals, and the residual U(VI) concentration was determined by ICP analysis. All experiments were conducted in triplicate to ensure reproducibility.

The adsorption capacity at time t (q_t, mg g^{-1}) was calculated using Eq. (1):

$$q_t = (C_0 - C_t) \times V / (1000 \times M) \quad (1)$$

where C_0 and C_t (mg L^{-1}) represent the initial and time-dependent uranium concentrations., V (L) is the solution volume, and M (g) is the mass of the adsorbent.

Adsorption kinetic models

To elucidate the rate-controling steps and adsorption mechanism three kinetic models—pseudo-first-order, pseudo-second-order, and intraparticle diffusion—were applied to fit the experimental data.

The Pseudo-first-order model assumes that the rate of site occupation is proportional to the number of unoccupied sites, typically describing **physisorption** governed by weak van der Waals forces (Eq. (2)):

$$\mathrm{Ln}\,(q_e - q_t) = \mathrm{Ln}\,qe - k_1 t \quad (2)$$

where q_t and q_e (mg g^{-1}) denote the adsorption capacities at time t and equilibrium, respectively, and k_1 (min^{-1}) is the pseudo-first-order rate constant.

The pseudo-second-order model assumes that the adsorption rate is proportional to the square of the number of unoccupied sites and **chemisorption** involving electron sharing or exchange is the rate limiting step (Eq. (3)):

$$t/q_t = 1/k_2 q_e^2 + t/q_e \quad (3)$$

where k_2 (g mg^{-1} min^{-1}) represent the pseudo-second-order rate constant.

The intraparticle diffusion model (Eq. (4)) proposed by Weber and Morris was also applied to identify the contribution of pore diffusion:

$$q_t = k_{id} t^{0.5} + C \quad (4)$$

where k_{id} (mg g^{-1} $min^{-0.5}$) is the intraparticle diffusion rate constant, and C (mg g^{-1}) corresponds the boundary layer effect. A line passing through the origin indicates pure intraparticle diffusion control, whereas multilinearity suggests a multiple stage adsorption process involving both surface adsorption and internal diffusion.

Adsorption isotherm models

Adsorption isotherms describe the relationship between the equilibrium concentration of adsorbate (C_e) and the amount adsorbed (q_e) at constant temperature. They provide insights into the adsorption mechanism, surface properties, and affinity of the adsorbent toward the adsorbate [32].

Two commonly used isotherm models—Langmuir and Freundlich—were employed to analyze the equilibrium data of U(VI) adsorption on SAN-NFs and SAN-HNFs.

The Langmuir model (Eq. (5)) assumes that adsorption occurs at specific homogeneous sites on the adsorbent surface, forming a monolayer of adsorption on a homogeneous surface with identical binding sites and no interaction between adsorbed molecules [33]:

$$C_e/q_e = C_e/q_m + 1/K_L q_m \quad (5)$$

where Ce is the equilibrium concentration (mg L^{-1}), qm (mg g^{-1}) is the maximum monolayer adsorption capacity, and K_L (L mg^{-1}) is the Langmuir constant representing the affinity of the binding sites.

The Freundlich model (Eq. (6)) is an empirical equation describing adsorption on heterogeneous surfaces with sites of varying energies, allowing multilayer adsorption:

$$log\ q_e = logK_f + 1/n\ logC_e \quad (6)$$

where the K_f *and n are the* Freundlich constants representing adsorption capacity and adsorption intensity (surface heterogenety), respectively.

Results and discussion

Optimization of SAN-NF Production

The production parameters of SAN nanofibers (SAN-NFs) were systematically optimized by varying polymer concentration (30–60 wt%), needle size (22G–30G), rotation speed (4000–6000 rpm), and nozzle-to-collector distance (10–20 cm). Fiber formation was observed only at polymer concentrations ≥55%, indicating a critical threshold for continuous fiber generation and stable morphology (Table 1).

Under optimal conditions—55% SAN concentration, 27G needle, 5000 rpm rotational speed, and 15 cm distance—uniform nanofibers with an average diameter of approximately 470 nm were obtained (Fig. 1). At lower polymer concentrations, droplets formation occurred due to insufficient chain entanglement. Both excessively high and low rotational speeds, as well as suboptimal collector distances, led to thicker or irregular fibers. Moreover, the use of finer needles (e.g., 30G) resulted in frequent clogging due to the high viscosity of the SAN solution.

Table 1 Evaluation of effective parameters in SAN-NF production by FS method.

SAN Concentration (%)	**The needles size (Gauge)**	**Rate Spin (rpm)**	**The nozzle-collector distance (cm)**	**Output**
30,40,45,50	22,24,27,30	5000	15	No fiber
55	22,30	5000	15	No fiber
	27			Nanofiber (470 nm)
	24			Nanofiber (644nm)
55	27	4000	15	Nanofiber (960 nm)
		6000		Nanofiber (868nm)
		5000	10	Nanofiber (910 nm)
			20	Nanofiber (885 nm)
60	27	5000	15	Nanofiber (900nm)

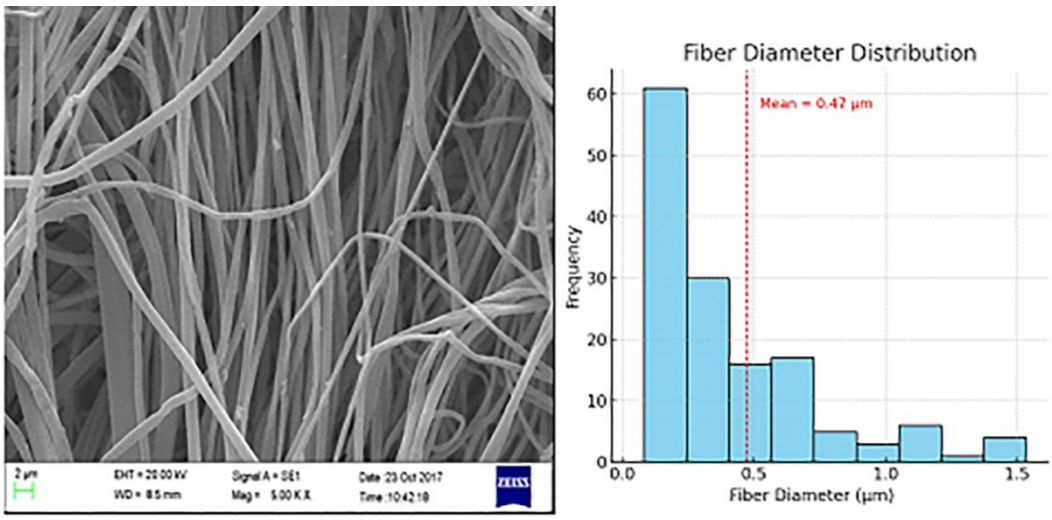


Fig. 1 Left: SEM image of optimized SAN nanofibers (SAN-NFs). Right: Histogram of fiber diameter distribution.

Optimization of SAN-HNF Production

The optimized parameters from SAN-NF fabrication were used as the starting conditions for SAN hollow nanofiber (SAN-HNF) production. however, the higher viscosity of the SAN/mineral oil emulsion prevented fiber formation with a 27G needle, necessitating the use of a 24G needle for successful spinning (Table 2).

The volume ratio of SAN solution to mineral oil played a crucial role in core-shell structure formation. Hollow fibers were obtained only at a 50:50 ratio; lower SAN content resulted in incomplete shell formation or absence of fibers. Cross-sectional SEM images (Fig. 2) confirmed the formation of hollow fibers with slightly off-centered cores and additional porosity.

While such off-centered morphology may be further refined in future work by introducing emulsion stabilizers or co-solvents, the presence of secondary porosity enhances the accessibility of adsorption sites, which is advantageous for adsorption applications.

Table 2 Effect of needle diameter and SAN/mineral oil ratio on SAN-HNF production by emulsion FS (SAN concentration = 55%, rotation speed = 5000 rpm, nozzle-collector distance = 15 cm, hexane incubation = 24 h).

Volume ratio (SAN/ oil)	The needles size (Guage)	Output
50:50	27	No fiber
50:50	24	Hollow fiber
40:60	24	Solid fiber
30:70	24	No fiber

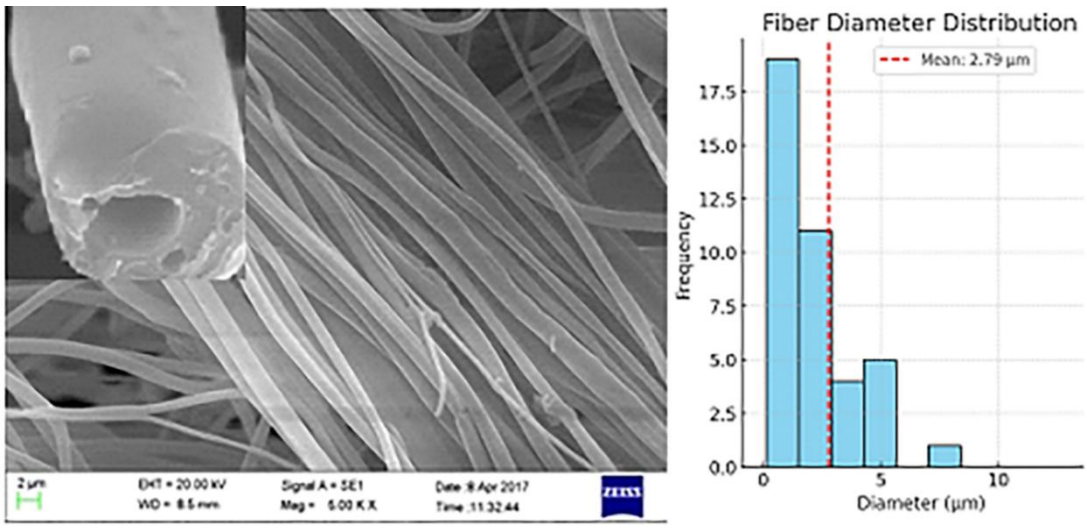
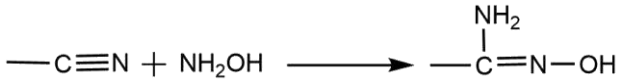


Fig. 2 Left: SEM image and cross-section of SAN-HNFs. Right: Fiber diameter distribution histogram.

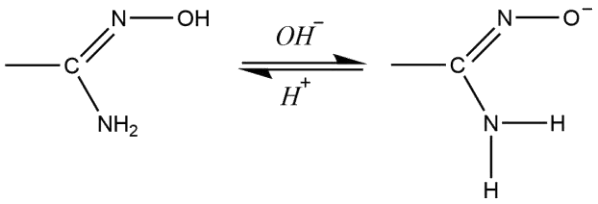
Amidoximation of Nanofibers

Amidoximation was carried out to introduce functional amidoxime groups capable of chelation uranium ions. The reaction proceeded through the nucleophilic addition of hydroxylamine to the nitrile groups present in SAN, converting -C≡N- into $–C(NH_2)=NOH$ functionalities (Scheme 3).

Subsequent alkaline treatment further enhanced adsorption capacity by deprotonating hydroxyl groups, which improved their affinity toward UO_2^{2+} ions through electrostatic attraction and coordination (Scheme 4) [34].



Scheme 3 Conversion of nitrile groups to amidoxime functional groups.



Scheme 4 Enhanced adsorption capacity of amidoxime groups after alkalization.

FT-IR Characterization

FT-IR analysis verified the successful amidoximation of both SAN-NFs and SAN-HNFs. The disappearance of the characteristic nitrile peak at 2240 cm^{-1}, along with the emergence of new absorption bands at 1650 cm^{-1} (C=N stretching) and 940 cm^{-1} (N–O stretching), confirmed the formation of amidoxime groups (Fig. 3).

This spectral transformation validates the chemical modification of SAN fibers and the introduction of functional groups responsible for uranium binding.

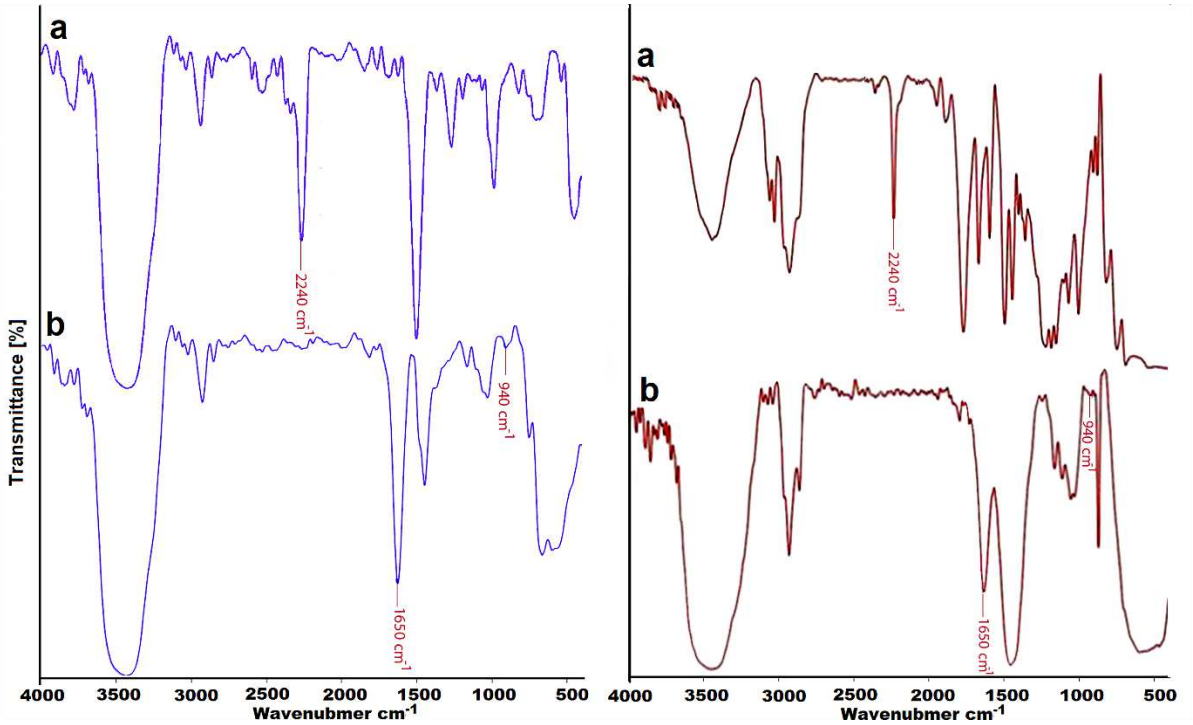


Fig. 3 FT-IR spectra of SAN-NFs (left) and SAN-HNFs (right): (a) before and (b) after the amidoximation.

Uranium Adsorption Performance

Effect of contact time

The effect of contact time on uranium adsorption was investigated to determine the adsorption rate and equilibrium behavior of U(VI) ions on amidoximated SAN-NFs and SAN-HNFs. As illustrated in Fig. 4, the adsorption capacity (q_t) increased rapidly during the initial stage of the process, particularly within the first 60–90 min, which can be attributed to the abundance of readily accessible amidoxime functional groups on the fiber surfaces.

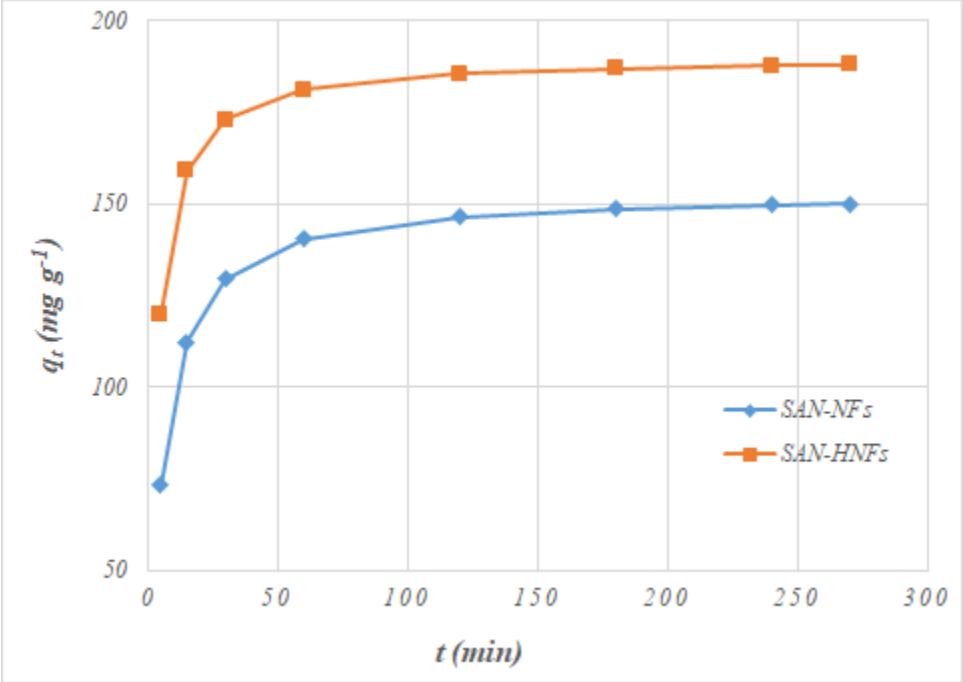


Fig. 4 Effect of contact time on U(VI) adsorption onto amidoximated SAN-NFs and SAN-HNFs.

With increasing contact time, the adsorption rate gradually decreased as active sites became progressively occupied, and equilibrium was reached after approximately 180 min for SAN-HNFs and 240 min for SAN-NFs. The shorter equilibrium time observed for SAN-HNFs clearly indicates a faster mass transfer process, which is mainly associated with their hollow interior structure. The hollow morphology provides a larger accessible surface area and shorter diffusion pathways for UO_2^{2+} ions, thereby facilitating more efficient utilization of the available adsorption sites.

This adsorption behavior can be described as a two-phase process consisting of an initial rapid uptake stage followed by a slower approach to equilibrium. Such behavior is characteristic of chemisorption-dominated systems, in which strong surface complexation between amidoxime groups and uranyl ions occurs at the early stage, while intrafiber diffusion and site saturation govern the later stage of adsorption.

A comparison with some previously reported amidoxime-based fibrous adsorbents (Table 3) further highlights the favorable time-dependent performance of SAN-HNFs. Although some composite fibrous adsorbents, such as electrospun PU–PAO nanofibers and PAN–GO nanofibers, exhibit higher maximum adsorption capacities, these enhanced performances are largely attributed to the presence of additional active components and, in some cases, operation under very high initial uranium concentrations. In contrast, the SAN-HNFs developed in this work demonstrate high adsorption efficiency within a moderate and practically relevant uranium concentration range (10–200 mg L^{-1}), while reaching adsorption equilibrium within a relatively short contact time. Despite being composed solely of amidoximated styrene–acrylonitrile copolymer without any inorganic or carbonaceous additives, the SAN-HNFs show competitive adsorption kinetics and capacity. In SAN, only the polyacrylonitrile segments are converted into amidoxime groups and actively participate in uranium binding, whereas the styrene units do not contribute directly to adsorption. Nevertheless, the optimized hollow architecture of SAN-HNFs effectively compensates for this intrinsic limitation by enhancing mass transfer efficiency and reducing diffusion resistance. Overall, the results demonstrate that the hollow amidoximated SAN nanofibers provide an advantageous balance between adsorption rate, equilibrium time, and adsorption capacity, making them promising candidates for practical uranium removal applications.

Table 3 Comparison of uranium adsorption capacities of SAN-HNFs with some amidoxime-based fibrous adsorbents.

No.	Adsorbent	q_{max} (mg g^{-1})	Optimal pH	Adsorption equilibrium time (h)	Reference
1	SAN-HNF	190	4.0	3	this work
2	SAN-NF	153	4.0	4	this work

3	PAO- cellulose fiber	52.9	5.0	5	[35]
4	Electrospun PU-PAO composite nanofibers	435	4.1	4	[36]
5	PAO- ultra-high molecular weight polyethylene fibers	99	4	12	[37]
6	PAO-polypropylene nanofibers	83	4	1	[38]
7	PAO-GO Nanofibers	345	5	1.5	[39]

278

279 Effect of pH

280 The adsorption behavior of amidoximated SAN-NFs and SAN-HNFs was investigated at
281 various pH values. As shown in Fig. 5, the adsorption capacity increased with increasing
282 pH, reaching a maximum at pH 4, beyond which it decreased.

283 At this optimal pH, the maximum adsorption capacities were 153 mg g^{-1} for amidoximated
284 SAN-NFs and 190 mg g^{-1} for SAN-HNFs, corresponding to a 24% improvement for the
285 hollow fibers. The enhanced performance of SAN-HNFs is attributed to their greater
286 internal porosity and larger effective surface area, which facilitates mass transfer and
287 provide additional active sites for uranium binding.

288 At pH < 4, of The amidoxime groups become protonated, weakening their coordination
289 ability toward UO_2^{2+} ions. At pH > 4, hydrolysis of uranium species forms soluble or
290 colloidal hydroxide complexes, thereby reducing the concentration of free uranyl ions
291 available for adsorption.

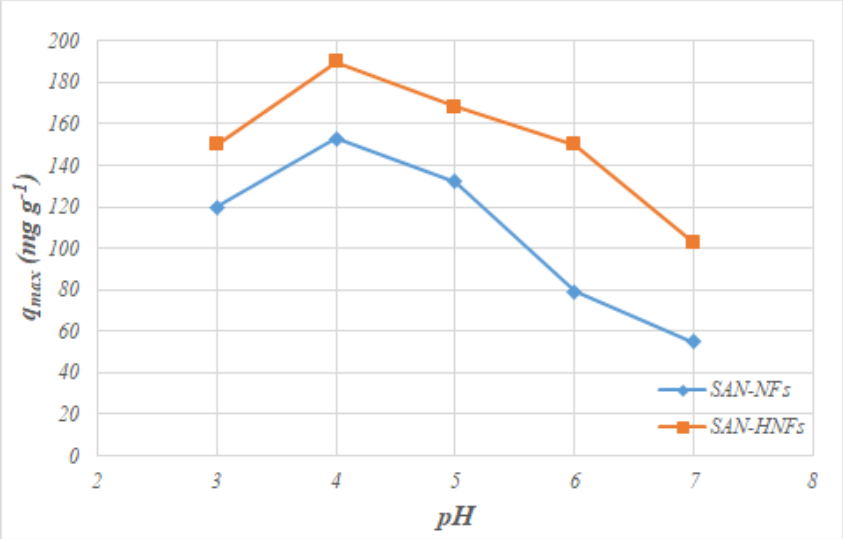


Fig. 5 *Effect of pH on uranium adsorption by SAN-NFs and SAN-HNFs.*

Adsorption Kinetics

The adsorption kinetics of UO_2^{2+} ions onto amidoximated SAN-NFs and SAN-HNFs were analyzed using pseudo-first-order and pseudo-second-order models. The correlation coefficients (R^2) revealed that the pseudo-second-order model provided a significantly better fit ($R^2 = 1$) compared to the pseudo-first-order model ($R^2 \leq 0.96$). This indicates that the adsorption process is predominantly governed by chemisorption involving electron sharing or exchange between amidoxime groups and UO_2^{2+} ions (Fig. 6).

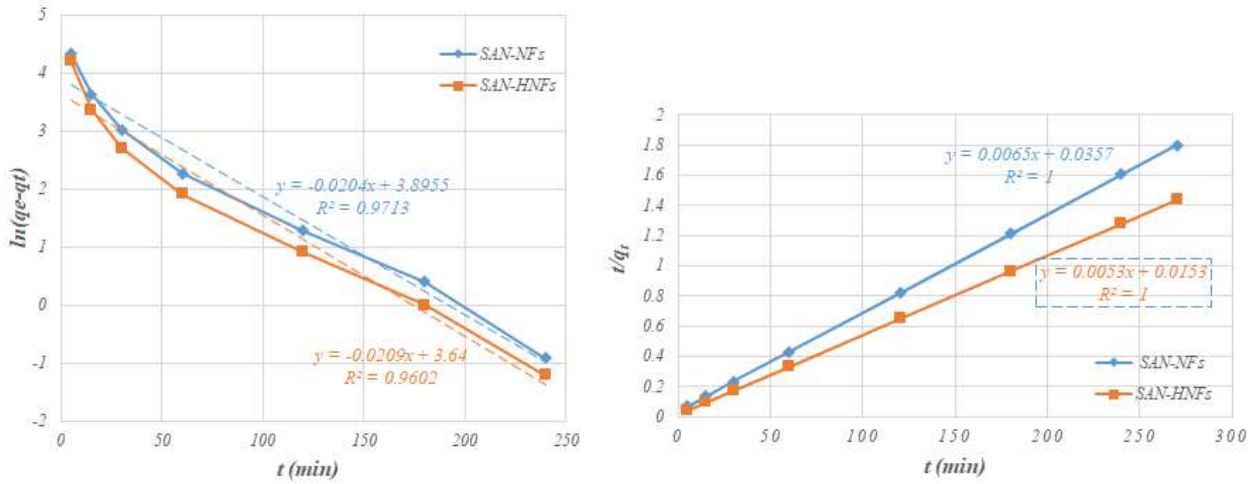


Fig. 6 Pseudo-first-order and pseudo-second-order kinetic plots for U(VI) adsorption on SAN-NFs and SAN-HNFs.

The intraparticle diffusion plots (Fig. 7) displayed two distinct linear regions for both adsorbents. The first stage corresponds to rapid external surface adsorption, followed by a second slower stage attributed to intraparticle diffusion into the inner pores of the fibers. The multilinearity confirms a **two-step adsorption process**, where surface adsorption dominates the initial stage and diffusion limits the later stage.

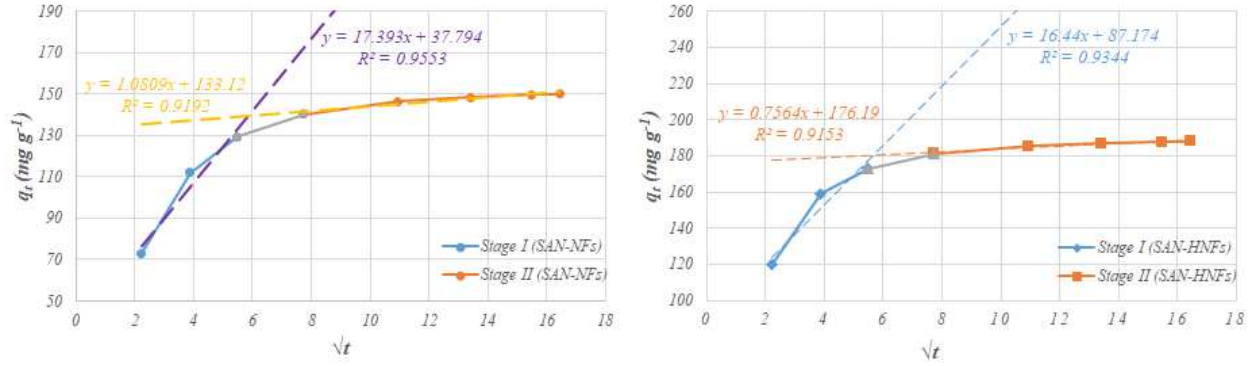


Fig. 7 Intraparticle diffusion plots *for U(VI) adsorption on SAN-NFs and SAN-HNFs.*

A summary of the kinetic parameters obtained from all models is presented in Table 4.

Table 4 Kinetic parameters for U(VI) adsorption on amidoximated SAN-NFs and SAN-HNFs.

Model	Parameter	SAN-NFs	SAN-HNFs

	q_e,exp (mg g^{-1})	153	190
Pseudo-first-order	q_e,calc (mg g^{-1})	49.18	38.09
	k_1 (min^{-1})	0.020	0.021
	R^2	0.97	0.96
Pseudo-second-order	q_e,calc (mg g^{-1})	154	189
	k_2 (g mg^{-1} min^{-1})	1.18×10^{-3}	1.84×10^{-3}
	R^2	1	1
Intraparticle diffusion (Stage I)	k_id_1 (mg g^{-1} $min^{-0.5}$)	17.39	16.44
	C_1 (mg g^{-1})	37.79	87.17
	R^2	0.95	0.93
Intraparticle diffusion (Stage II)	k_id_2 (mg g^{-1} $min^{-0.5}$)	1.08	0.76
	C_2 (mg g^{-1})	133.12	176.19
	R^2	0.92	0.91

315

316 Adsorption Isotherms

317 Adsorption equilibrium data were analyzed using the Langmuir and Freundlich isotherm
318 models. The corresponding linear plots are shown in Fig. 8, and the calculated model
319 parameters and correlation coefficients are summarized in Table 5.

320 The Langmuir model provides an excellent fit for both adsorbents (R^2 = 0.9996 and
321 0.9995), indicating monolayer adsorption on a homogeneous distribution of active sites.
322 The calculated maximum monolayer capacities are for SAN-NF and for SAN-HNF,
323 showing a substantial improvement (~22.7%) for the hollow fibers. The higher K_L value
324 for SAN-HNF (0.1726 L mg^{-1} vs. 0.1035 L mg^{-1}) further indicates a stronger affinity of
325 SAN-HNF toward U(VI).

326 Although the Freundlich model also fits reasonably well (especially for SAN-HNF, R^2 =
327 0.9928), its lower R^2 values relative to Langmuir and the near-unity values (but>1) of the
328 Freundlich constant n suggest favorable adsorption with moderately uniform surface

energetics, while the superior fitting of the Langmuir model indicates monolayer adsorption behavior.

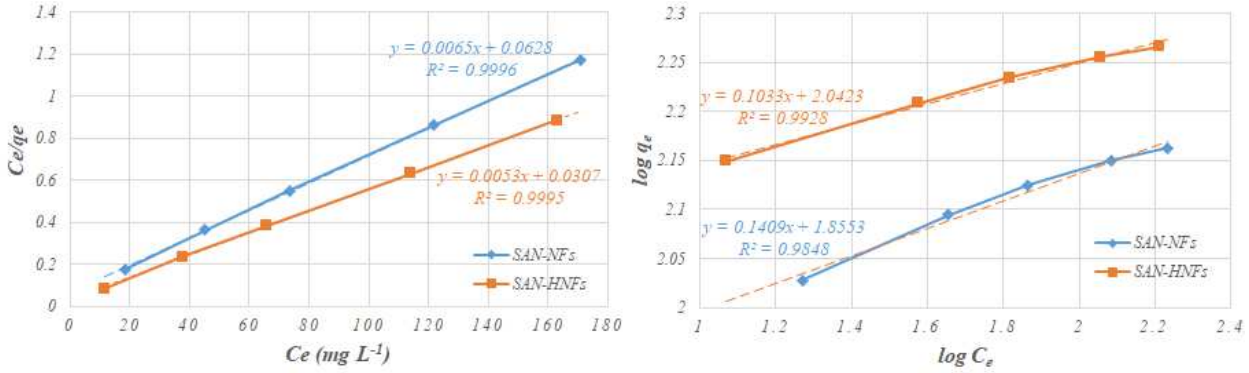


Fig. 8 Adsorption isotherms of UO_2^{2+} on amidoximated SAN-NFs and SAN-HNFs.

Table 5 Isotherm parameters for U(VI) adsorption on amidoximated SAN-NFs and SAN-HNFs

Model	Parameter	SAN-NF	SAN-HNF
Langmuir (linear)	q_m (mg g^{-1})	154	189
	K_L	0.1035	0.1726
	R^2	0.9996	0.9995
Freundlich (linear)	K_f	71.8	110.2
	n	7.10	9.68
	R^2	0.9848	0.9928

Effect of Initial Concentration

The influence of the initial uranium concentration (C_0) on the adsorption capacity was investigated in the range of 10–300 mg L^{-1}, at constant pH (4.0) and adsorbent dosage of 0.2 g L^{-1}. As shown in *Fig. 9,* adsorption capacity (q_e) increased with increasing C_0 due to a higher mass transfer driving force and greater collision probability between U(VI) ions and active sites.

For SAN-NFs, q_e increased from approximately 53 mg g^{-1} at 10 mg L^{-1} to 145 mg g^{-1} at 200 mg L^{-1}, approaching saturation at higher concentrations. Similarly, SAN-HNFs

exhibited a continuous increase from 75 mg g^{-1} at 10 mg L^{-1} to 185 mg g^{-1} at 200 mg L^{-1}, clearly demonstrating their superior uptake ability.

The sharp increase in q_e up to approximately 100 mg L^{-1} suggests that a large number of amidoxime functional groups were still available for U(VI) binding. However, at higher concentrations (above 200 mg L^{-1}), the adsorption capacity tended to level off, indicating that most of the active sites became occupied and the system approached equilibrium. This saturation behavior corresponds well with the Langmuir isotherm, which assumes monolayer coverage of adsorbate molecules onto a finite number of identical sites. Therefore, while increasing uranium concentration enhances adsorption initially, the plateau observed at higher concentrations reflects the limitation imposed by the finite surface area and the number of available binding sites.

Overall, the SAN-HNFs exhibited the higher equilibrium capacities clearly demonstrates that the hollow structure provides a larger accessible surface area and more efficient utilization of functional groups under increasing initial concentrations.

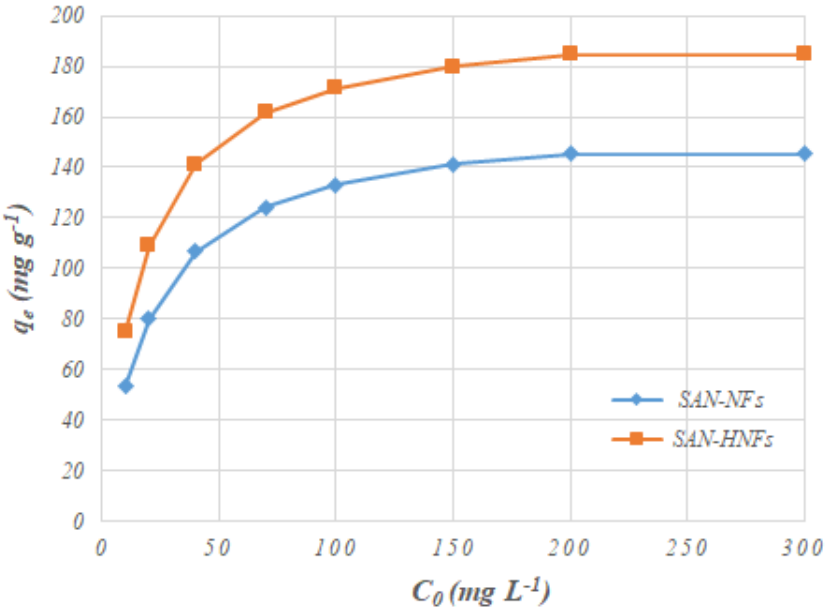


Fig. 9 Effect of initial U(VI) concentration on adsorption capacity for SAN-NFs and SAN-HNFs.

Conclusion

A novel emulsion-based forcespinning (FS) method was successfully developed to fabricate hollow amidoxime-functionalized styrene–acrylonitrile nanofibers (SAN-HNFs). The hollow core architecture provided enhanced surface accessibility and faster mass transfer compared to solid SAN nanofibers (SAN-NFs). As a result, SAN-HNFs exhibited superior uranium adsorption performance, achieving a maximum adsorption capacity of 190 mg g^{-1}, which was approximately 1.4 times higher than that of solid fibers under identical conditions.

The adsorption kinetics followed a pseudo-second-order model, confirming that chemisorption was the dominant mechanism, while the equilibrium data fitted well with the Langmuir isotherm, indicating monolayer adsorption on homogeneous active sites. The fibers maintained high efficiency within moderate uranium concentration ranges (10–200 mg L^{-1}), which are representative of industrial wastewater levels.

This work demonstrates, for the first time, the effectiveness of emulsion FS for producing hollow SAN nanofibers with high adsorption capacity and chemical stability. Owing to its simplicity, scalability, and reduced solvent use, the method holds great promise for the large-scale production of nanofibrous adsorbents for uranium recovery and environmental remediation.

FUNDING

This research did not receive any specific grant from funding agencies in the public, commercial, or not-for-profit sectors.

References

1. Ren L, Pandit V, Elkin J, Denman T, Cooper JA, Kotha SP (2013) Large-scale and highly efficient synthesis of micro- and nano-fibers with controlled fiber morphology by centrifugal jet spinning for tissue regeneration. *Nanoscale* 5:2337–2345. https://doi.org/10.1039/c3nr33423f

2. Valipouri A, Hosseini Ravandi SA, Pishevar AR (2013) A novel method for manufacturing nanofibers. *Fibers Polym* 14:941–949. https://doi.org/10.1007/s12221-013-0941-6

3. Lu Y, Li Y, Zhang S (2013) Parameter study and characterization for polyacrylonitrile nanofibers fabricated via centrifugal spinning process. *Eur Polym J* 49:3834–3845. https://doi.org/10.1016/j.eurpolymj.2013.09.017

4. Sarkar K, Gomez C, Zambrano S (2010) Electrospinning to forcespinning. *Mater Today* 13:12–14. https://doi.org/10.1016/S1369-7021(10)70199-1

5. Hammami MA, Krifa M, Harzallah O (2014) Centrifugal force spinning of PA6 nanofibers–processability and morphology of solution-spun fibers. *J Text Inst* 105:637–647. https://doi.org/10.1080/00405000.2013.842680

6. Obregon N, Agubra V, Pokhrel M, Campos H, Flores D, De la Garza D, Lozano K (2016) Effect of polymer concentration, rotational speed, and solvent mixture on fiber formation using forcespinning. *Fibers* 4:20. https://doi.org/10.3390/fib4020020

7. Zhang X, Lu Y (2014) Centrifugal spinning: An alternative approach to fabricate nanofibers at high speed and low cost. *Polym Rev* 54:677–701. https://doi.org/10.1080/15583724.2014.935858

8. Mahalingam S, Edirisinghe M (2013) Forming of polymer nanofibers by a pressurized gyration process. *Macromol Rapid Commun* 34:1134–1139. https://doi.org/10.1002/marc.201300339

9. Padron S, Fuentes A, Caruntu D (2013) Lozano K. Experimental study of nanofiber production through forcespinning. *J Appl Phys* 113:024318. https://doi.org/10.1063/1.4769886

10. McEachin Z, Lozano K (2012) Production and characterization of polycaprolactone nanofibers via forcespinningTM technology. *J Appl Polym Sci* 126:473–479. https://doi.org/10.1002/app.36843

11. Vazquez B, Vasquez H, Lozano K (2012) Preparation and characterization of polyvinylidene fluoride nanofibrous membranes by forcespinning. *Polym Eng Sci* 52:2260–2265. https://doi.org/10.1002/pen.23169

12. Maul J, Frushour BG, Kontoff JR, Eichenauer H, Ott KH, Schade C (2012) Polystyrene and styrene copolymers. In: *Ullmann's Encyclopedia of Industrial Chemistry*. 5rd edn. VCH, Weinheim p. 475–522

13. Kim JR, Hudson SD, Jamieson AM, Manas-Zloczower I, Ishida H (2000) Influence of segmental swelling of an asymmetric block copolymer on the morphology of melt-mixed immiscible polymer blends. *Polymer* 41:9163–9168. https://doi.org/10.1016/S0032-3861(00)00283-4

14. Senthil T, Anandhan S (2014) Fabrication of styrene–acrylonitrile random copolymer nanofiber membranes from N,N-dimethylformamide by electrospinning. J Elastom Plast 46:1–20. https://doi.org/10.1177/0095244313514987

15. Senthil T, Anandhan S (2013) Solution electrospinning of styrene-acrylonitrile random copolymer from dimethyl sulfoxide. *Int J Plast Technol* 17:123–138. https://doi.org/10.1007/s12588-013-9053-9

16. Bandegi A, Moghbeli MR (2018) Effect of solvent quality and humidity on porous formation and oil absorbency of SAN electrospun nanofibers. J Appl Polym Sci 135:45586. https://doi.org/10.1002/app.45586

17. Mohamud H, Ivanov P, Russell BC, Regan PH, Ward NI (2018) Selective sorption of uranium from aqueous solution by graphene oxide-modified materials. *J Radioanal Nucl Chem* 316:839–848. https://doi.org/10.1007/s10967-018-5741-4

18. Xu S, Zhang C, Zhao X, Yang J, Zhang X, Wang J (2009) Removal of uranium (VI) from aqueous solution by adsorption of hematite. *J Environ Radioact* 100:162–166. https://doi.org/10.1016/j.jenvrad.2008.09.008

19. Villalobos-Rodriguez R, Montero-Cabrera ME, Esparza-Ponce HE, Herrera-Peraza EF, Ballinas-Casarrubias ML (2012) Uranium removal from water using cellulose triacetate membranes added with activated carbon. *Appl Radiat Isot* 70:872–881. https://doi.org/10.1016/j.apradiso.2012.01.017

20. Bakatula EN, Mosai AK, Tutu H (2015) Removal of uranium from aqueous solutions using ammonium-modified zeolite. *S Afr J Chem* 68:165–171. https://doi.org/10.17159/0379-4350/2015/v68a23

21. Martins M, Faleiro ML, Chaves S, Tenreiro R, Santos E, Costa MC (2010) Anaerobic bio-removal of uranium (VI) and chromium (VI): Comparison of microbial community structure. *J Hazard Mater* 176:1065–1072. https://doi.org/10.1016/j.jhazmat.2009.11.149

22. Majdan M, Pikus S, Gajowiak A, Sternik D, Zięba E (2010) Uranium sorption on bentonite modified by octadecyl trimethyl ammonium bromide. *J Hazard Mater* 184:662–670. https://doi.org/10.1016/j.jhazmat.2010.08.089

23. Van Suc N, Ly HTY (2011) Adsorption of U(VI) from aqueous solution onto modified chitosan. *Int J Chemtech Res* 3:1993–2002

24. Gregorio C (2005) Recent development in polysaccharide-based materials used as adsorbents in wastewater treatment. *Prog Polym Sci* 30:38–70. https://doi.org/10.1016/j.progpolymsci.2004.11.002

25. Wan Ngah WS, Endua CS, Mayanar R (2002) Removal of copper (II) ions from aqueous solution onto chitosan and cross-linked chitosan beads. *React Funct Polym* 50:181–190. https://doi.org/10.1016/S1381-5148(01)00113-4

26. Xu X, Zhuang X, Chen X, Wang X, Yang L, Jing X (2006) Preparation of core-sheath composite nanofibers by emulsion electrospinning. *Macromol Rapid Commun* 27:1637–1642. https://doi.org/10.1002/marc.200600384

27. Qu H, Wei S, Guo Z (2013) Coaxial electrospun nanostructures and their applications. *J Mater Chem A* 1:11513–11528. https://doi.org/10.1039/c3ta12390a

28. Moghe AK, Gupta BS (2008) Co-axial electrospinning for nanofiber structures: Preparation and applications. *Polym Rev* 48:353–377. https://doi.org/10.1080/15583720802022257

29. Ren L, Ozisik R, Kotha SP, Underhill PT (2015) Highly efficient fabrication of polymer nanofiber assembly by centrifugal jet spinning: Process and characterization. *Macromolecules* 48:2593–2602. https://doi.org/10.1021/acs.macromol.5b00292.

30. McClellan P, Landis WJ (2016) Recent applications of coaxial and emulsion electrospinning methods in the field of tissue engineering. *J Biomed Mater Res A* 104(4):987–1004. https://doi.org/10.1089/biores.2016.0022

31. Yarin RL (2011) Coaxial electrospinning and emulsion electrospinning of core-shell fibers. *Polym Adv Technol* 22:310–317. https://doi.org/10.1002/pat.1781

32. Ogunmodede OT, Ojo AA, Adewole E, Adebayo OL (2015) Adsorptive removal of anionic dye from aqueous solutions by mixture of kaolin and bentonite clay: characteristics, isotherm, kinetic and thermodynamic studies. Int J Energy Environ 6:147–153

33. Belhamdi B, Merzougui Z, Trari M, Addoun A (2016) A kinetic, equilibrium and thermodynamic study of L-phenylalanine adsorption using activated carbon based on agricultural waste. J Appl Res Technol 14:354–366. https://doi.org/10.22201/icat.16656423.2016.14.5.26

34. Masoumi A, Hemati K, Ghaemy M (2015) Structural modification of Acrylonitrile-Butadiene-Styrene waste as an efficient nano adsorbent for removal of metal ions from water: Isotherm, kinetic and thermodynamic study. *RSC Adv* 5:1735–44. https://doi.org/10.1039/C4RA10830B

35. Wang Y, Zhang Y, Li Q, Li Y, Cao L, Li W (2020) Amidoximated cellulose fiber membrane for uranium extraction from simulated seawater. Carbohydr Polym 245:116627. https://doi.org/10.1016/j.carbpol.2020.116627

36. Alemdar S, Bayramgil NP (2025) Preparation of polyacrylonitrile-based nanofiber mats by electrospinning for uranium recovery. J Chem Technol Biotechnol 100:2299–2308. https://doi.org/10.1002/jctb.70042

37. Xie CY, Jing SP, Wang Y, Lin X, Bao HL, Guan CZ, Jin C, Wang JQ (2017) Adsorption of uranium(VI) onto amidoxime-functionalized ultra-high molecular

503 weight polyethylene fibers from aqueous solution. Nucl Sci Tech 28:94.
504 https://doi.org/10.1007/s41365-017-0251-6

505 38. Ashrafi F, Firouzzare M, Ahmadi SJ, Sohrabi MR, Khosravi M (2019) Preparation
506 and modification of forcespun polypropylene nanofibers for adsorption of
507 uranium(VI) from simulated seawater. Ecotoxicol Environ Saf 186:109746.
508 https://doi.org/10.1016/j.ecoenv.2019.109746

509 39. Ashrafi F, Firouzzare M (2021) Preparation of forcespun amidoximated
510 polyacrylonitrile–graphene oxide nanofibers and evaluation of their uranium
511 uptake from aqueous media. Fibers Polym 22:3289–3297.
512 https://doi.org/10.1007/s12221-021-0133-8

513

514